Electronic Supporting Information

[^{1}H]/[^{2}H] discriminated bianthryl atropisotopomers: enantiospecific syntheses from BINOL and direct multi-spectroscopic analyses of their isotopic chirality

Florian Rigoulet,[a] Guillaume Dauvergne,[a] Jean-Valère Naubron,*[b,d] Philippe Lesot,*[c,d] Christie Aroulanda[c] and Yoann Coquerel*[a,d]

[a] *Aix Marseille Univ, CNRS, Centrale Med, ISM2, 13397 Marseille, France.*
[b] *Aix Marseille Univ, CNRS, Centrale Med, FSCM, 13397 Marseille, France.*
[c] *Université Paris-Saclay, CNRS UMR 8182, ICMMO, RMN en Milieu Orienté, Bât. 670, 17 avenue des Sciences, 91400, Orsay, France.*
[d] *Centre National de la Recherche Scientifique, CNRS, 3 rue Michel-Ange, 75016 Paris, France.*

E-mail: philippe.lesot@universite-paris-saclay.fr; yoann.coquerel@univ-amu.fr

Table of content

Section S1: Syntheses

S1.1. General materials and methods

Chemical reactions were carried out under an argon atmosphere in oven-dried reaction vessels in anhydrous solvents using syringes. All reagents were weighed and handled in air at room temperature unless otherwise mentioned, and all commercially available reagents were used as received. Anhydrous dichloromethane, diethyl ether, and toluene were dried by filtration over solid dehydrating agents using a commercial solvent purification system.

Commercially available d_4-furan (with ≥ 99% chemical purity and ≥ 98% isotopic purity) and trimethylsilylmethylmagnesium chloride solutions (1.0 M in Et_2O) were obtained from Merck. Commercially available trimethylsilylmethylmagnesium chloride solutions were systematically titrated prior to use by reactions (assumed quantitative) with benzaldehyde (99% chemical purity) in anhydrous diethyl ether at 25 °C: all freshly opened 100 mL bottles of the commercial reagent were confirmed 1.0 M.

The enantiomeric bis(aryne) synthetic equivalent (*aR*)-**11** (99% *ee*) and (*aS*)-**11** (>99% *ee*) were prepared in four steps and 77% yield from (*aR*)-BINOL (>99% *ee*) and (*aS*)-BINOL (>99% *ee*), respectively, as previously described.[1]

Normal phase thin layer chromatography analyses were carried out on Merck Kieselgel 60 F_{254} 0.2 mm plates, and reverse phase thin layer chromatography analyses were carried out on Macherey-Nagel Alugram RP-18 W UV254 plates. Visualization was accomplished using ultraviolet light (254 and/or 365 nm) and/or chemical staining with an ethanolic solution of para-anisaldehyde with sulphuric acid as appropriate.

Melting points were recorded using a Büchi Melting Point B-540 apparatus.

Standard (isotropic) NMR spectra were recorded in deuterated chloroform ($CDCl_3$) at 298 ± 3 K in 9.4 T or 11.7 T spectrometers using the residual nondeuterated solvent as an internal standard for ^{1}H NMR (δ = 7.26 ppm) and the deuterated solvent signal for ^{13}C NMR (δ = 77.16 ppm). Chemical shifts (δ) are expressed in ppm, coupling constants (*J*) in Hertz (Hz), and the classical abbreviations are used to describe the signal multiplicities. DEPT-135 was used to support assignments.

High resolution mass spectra (HRMS) were recorded in triplicate with three consistent measurements at the Spectropole (http://fr-chimie.univ-amu.fr/spectropole/) on a Waters Synapt G2 mass spectrometer apparatus using a positive electrospray ionization (ESI) source. The optimum 'found' value is reported.

S1.2. Results

Syntheses of (*aR*)-**9** and (*aS*)-**9**:

A round bottom flask equipped with a magnetic stirring bar containing the enantioenriched aryne precursor (*aR*)-**11** (99% *ee*, 100 mg, 0.125 mmol) was charged with 3 mL of anhydrous toluene. The toluene was evaporated in vacuo and this step was repeated twice to remove moisture. Then the flask was charged with 5 mL anhydrous Et_2O and d_4-furan (44 µL, 0.60 mmol) under an argon atmosphere. The suspension was cooled down to 0 °C and a 1.0 M solution of trimethylsilylmethylmagnesium chloride in diethyl ether (2.50 mL, 2.50 mmol) was added at this temperature over 4 hours using a

syringe pump. The reaction mixture was kept at 0 °C with stirring for an additional 12 h, and was hydrolyzed with water (10 mL). The aqueous and organic layers were separated, and the aqueous layer was extracted three time with EtOAc. The combined organic layers were washed with brine, dried over anhydrous Na_2SO_4, filtered and concentrated under reduced pressure to afford a colorless oil (40 mg).

This residue was transferred to a 25 mL round bottom flask equipped with a magnetic stirring bar, placed under an argon atmosphere and dissolved in anhydrous dichloromethane (2 mL). Then, solid NaI (90 mg, 0.60 mmol) and Me_3SiCl (76 µL, 0.60 mmol) were added at 25 °C, and stirring was turned on resulting in an immediate dark brown coloration of the solution. After 15 min at 25 °C, TLC analysis (normal phase) revealed a complete conversion, and saturated aqueous $NaHCO_3$ (10 mL) was added to the reaction mixture. The mixture was extracted three times with AcOEt (15 mL). The combined organic layers were washed with brine, dried over anhydrous Na_2SO_4, filtered and concentrated under reduced pressure to afford the crude product. Purification of this material by flash chromatography (40-63 µm silica gel) eluted with 50:1 pentane/ethyl ether afforded (*aR*)-**9** (25 mg, white solid) in 55% yield from (*aR*)-**11**.

Mp >360 °C (amorphous); **TLC** (normal phase, pentane/Et_2O = 10:1) R_f = 0.82; **HRMS** (ESI+) *m/z* calcd for $C_{28}H_{10}D_8Ag^+$ $[M+Ag]^+$ 469.0956, found 469.0947; **^{1}H NMR** (400 MHz, $CDCl_3$) δ 8.68 (s, 2H), 8.15 (d, *J* = 8.6 Hz, 2H), 7.44 (ddd, *J* = 9.0, 6.5, 1.2 Hz, 2H), 7.16–7.07 (m, 4H); **^{13}C{^{1}H} NMR** (126 MHz, $CDCl_3$) δ 133.2 (2C), 131.8 (2C), 131.7 (4C), 131.6 (2C), 128.7 (2CH), 128.2 (t, $^1J_{C\text{-}D}$ = 23.9 Hz, 2CD), 127.3 (2CH), 127.0 (2CH), 126.6 (t, $^1J_{C\text{-}D}$ = 25.2 Hz, 2CD), 125.9 (2CH), 125.4 (2CH), 125.4 (t, $^1J_{C\text{-}D}$ = 24.5 Hz, 2CD), 124.9 (t, $^1J_{C\text{-}D}$ = 25.0 Hz, 2CD).

Realizing the same experimental protocol from (*aS*)-**11** (>99% *ee*, 100 mg, 0.125 mmol), furnished 24 mg (53% yield) of (*aS*)-**9** as a white solid. The sample of (*aS*)-**9** was indistinguishable from the sample of (*aR*)-**9**.

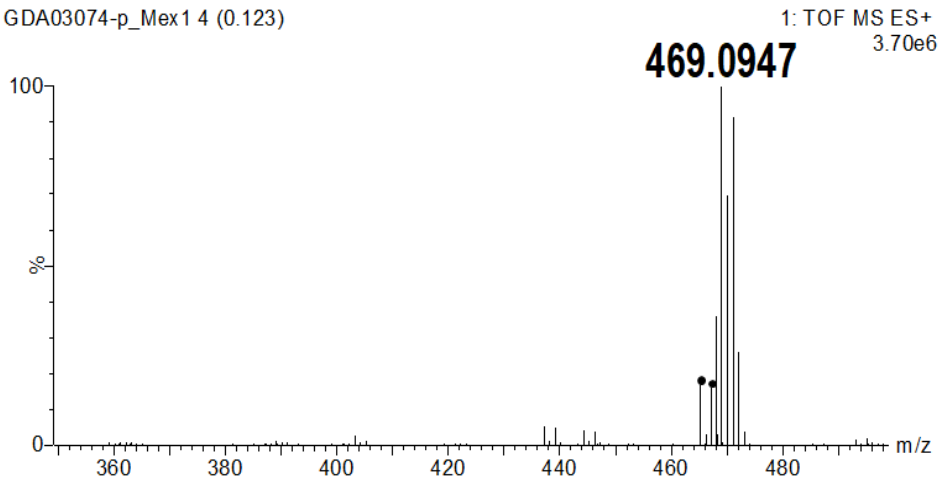

Figure S1. HRMS spectrum (ESI+) of (*aR*)-**9**. The detected ion is the $[M+Ag]^+$ adduct of formula $C_{28}H_{10}D_8Ag^+$ with calculated *m/z* = 469.0956. The two ions annotated with black dots were present in the analytical blank spectrum and thus are not derived from the analyte. The isotopic profile indicates that, in addition to the expected ion with *m/z* 469.1, the analyte contains a minor amount of a product that has *m/z* 468.1.

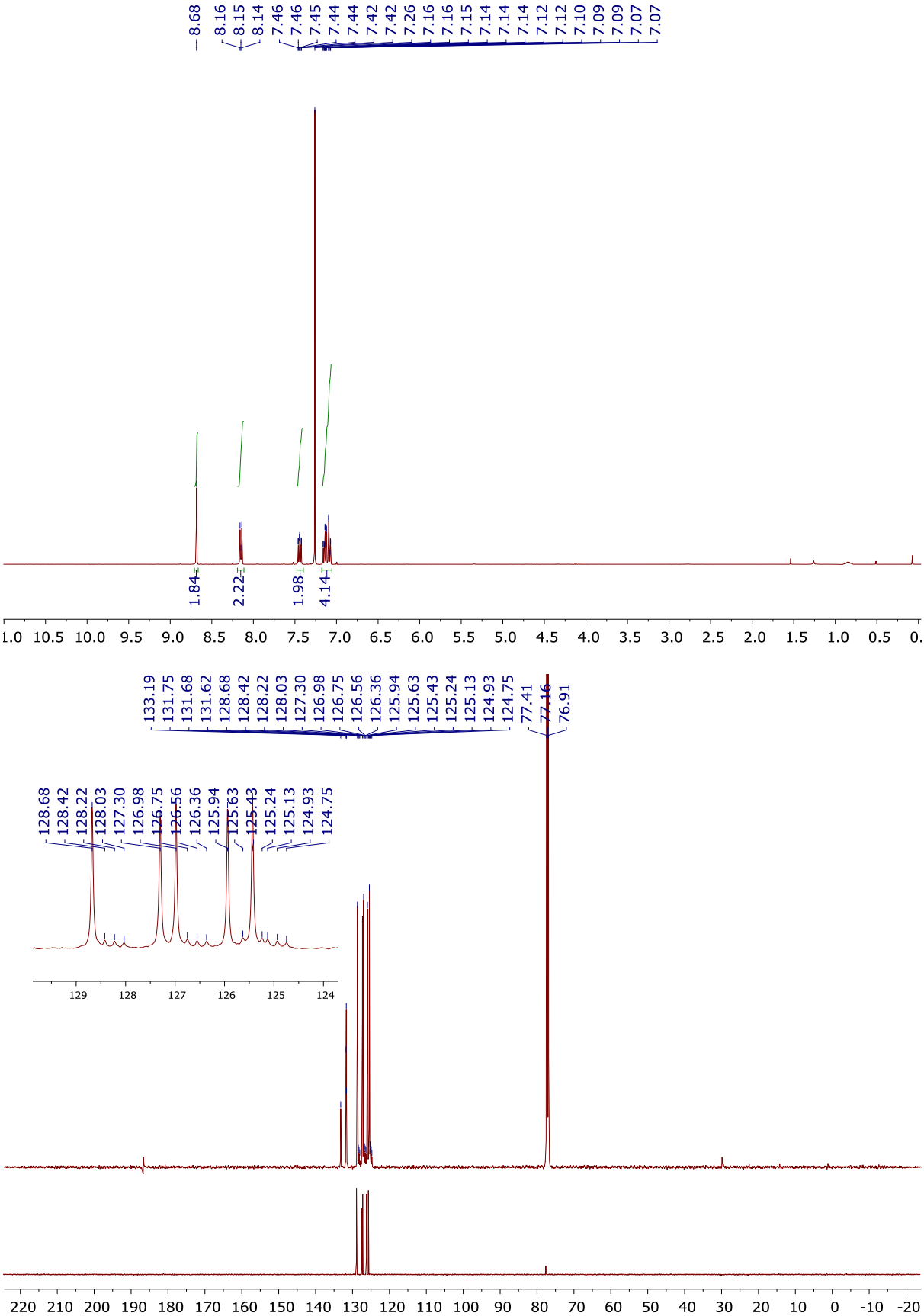

Figure S2. Top: ^{1}H NMR (500 MHz, $CDCl_3$) spectrum of (*aR*)-(**9**); bottom: $^{13}C\{^{1}H\}$ and DEPT-135 NMR (126 MHz, $CDCl_3$) spectra of (*aR*)-(**9**).

Syntheses of (*aS*)-**10** and (*aR*)-**10**:

A round bottom flask equipped with a magnetic stirring bar containing the enantioenriched aryne precursor (*aS*)-**11** (>99% *ee*, 400 mg, 0.499 mmol) was charged with 15 mL of anhydrous toluene. The toluene was evaporated in vacuo and this step was repeated twice to remove moisture. Then the flask was charged with 15 mL anhydrous Et_2O, d_4-furan (90 µL, 1.24 mmol) and 3,4-dibromofuran (320 mg, 1.42 mmol) under an argon atmosphere. The suspension was cooled down to 0 °C and a 1.0 M solution of trimethylsilylmethylmagnesium chloride in diethyl ether (10 mL, 10 mmol) was added at this temperature over 4 hours using a syringe pump. The reaction mixture was kept at 0 °C with stirring for an additional 12 h, and was hydrolyzed with water (40 mL). The aqueous and organic layers were separated, and the aqueous layer was extracted three time with EtOAc. The combined organic layers were washed with brine, dried over anhydrous Na_2SO_4, filtered and concentrated under reduced pressure to afford a light brown oil.
This residue was transferred to a 100 mL round bottom flask equipped with a magnetic stirring bar, placed under an argon atmosphere and dissolved in anhydrous dichloromethane (10 mL). Then, solid NaI (360 mg, 2.40 mmol) and Me_3SiCl (310 µL, 2.44 mmol) were added at 25 °C, and stirring was turned on resulting in an immediate dark brown coloration of the solution. After 15 min at 25 °C, TLC analysis (normal phase) revealed a complete conversion, and saturated aqueous $NaHCO_3$ (40 mL) was added to the reaction mixture. The mixture was extracted three times with AcOEt (60 mL). The combined organic layers were washed with brine, dried over anhydrous Na_2SO_4, filtered and concentrated under reduced pressure to afford the crude product. Purification of this material by reverse phase silica gel column chromatography (Polygoprep® 60-50 C18 from Macherey-Nagel, 10 g) eluted with methanol afforded first 16 mg of (*aS*)-**9** [9% yield from (*aS*)-**11**] followed by 28 mg of (*aS*)-**10** [11% yield from (*aS*)-**11**].

For (*aS*)-**10**: **Mp** = 278 °C (amorphous, decomposition); **TLC** (normal phase, pentane/ethyl acetate = 49:1) R_f = 0.29; **TLC** (reverse phase, methanol) R_f = 0.51; **HRMS** (ESI+) $[M+Ag]^+$ calcd for $C_{28}H_{12}D_4Br_2Ag^+$ = 622.8902, found 622.8904; **^{1}H NMR** (500 MHz, $CDCl_3$) δ 8.72 (s, 1H), 8.56 (s, 1H), 8.48 (s, 1H), 8.17 (d, *J* = 8.6 Hz, 1H), 8.12 (d, *J* = 8.6 Hz, 1H), 7.51–7.43 (m, 2H), 7.40 (s, 1H), 7.21–7.13 (m, 2H), 7.05–6.98 (m, 2H); **^{13}C{^{1}H} NMR** (126 MHz, $CDCl_3$) δ 133.2 (C), 132.8 (CH), 132.4 (C), 132.4 (C), 131.6 (2C), 131.6 (C), 131.6 (C), 131.5 (C), 131.2 (CH), 131.1 (C), 130.9 (C), 128.9 (CH), 128.7 (CH), 128.4 (t, $^1J_{C\text{-}D}$ = 24.6 Hz, CD), 128.0 (CH), 127.1 (CH), 126.9 (CH), 126.6 (CH), 126.5 (CH), 126.4 (CH), 126.2 (CH), 126.1 (t, $^1J_{C\text{-}D}$ = 25.1 Hz, CD), 125.6 (CH), 124.1 (t, $^1J_{C\text{-}D}$ = 25.4 Hz, CD), 122.5 (C), 122.0 (C), 1 C-D triplet resonance could not be observed due to signals overlapping.

Realizing the same experimental protocol from (*aR*)-**11** (99% *ee*, 400 mg, 0.499 mmol), furnished 27 mg (10% yield) of (*aR*)-**10** as a white solid. The sample of (*aR*)-**10** was indistinguishable from the sample of (*aS*)-**10**.

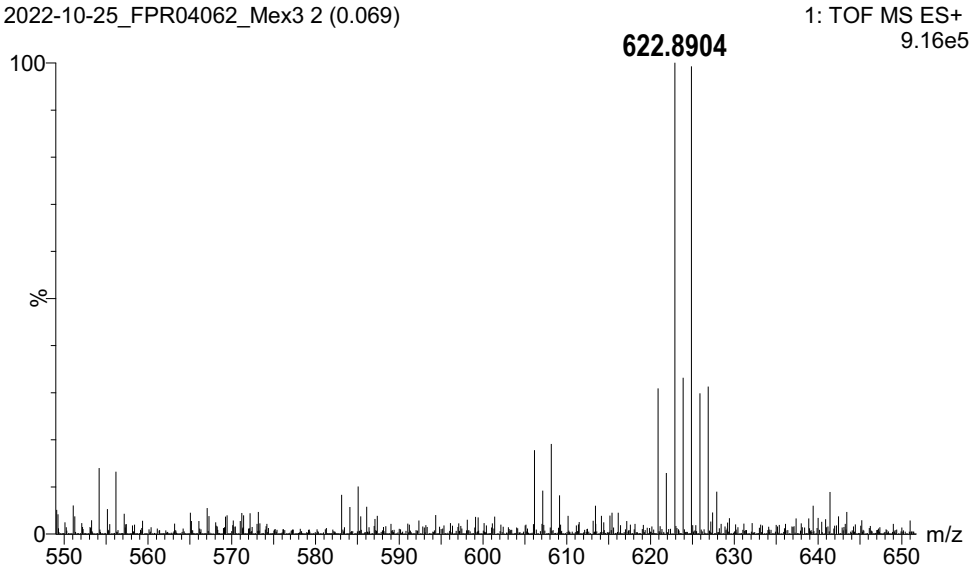

Figure S3. HRMS spectrum (ESI+) of (aS)-**10**. The detected ion is the $[M+Ag]^+$ adduct of formula $C_{28}H_{12}D_4Br_2Ag^+$ with calculated *m/z* = 622.8902.

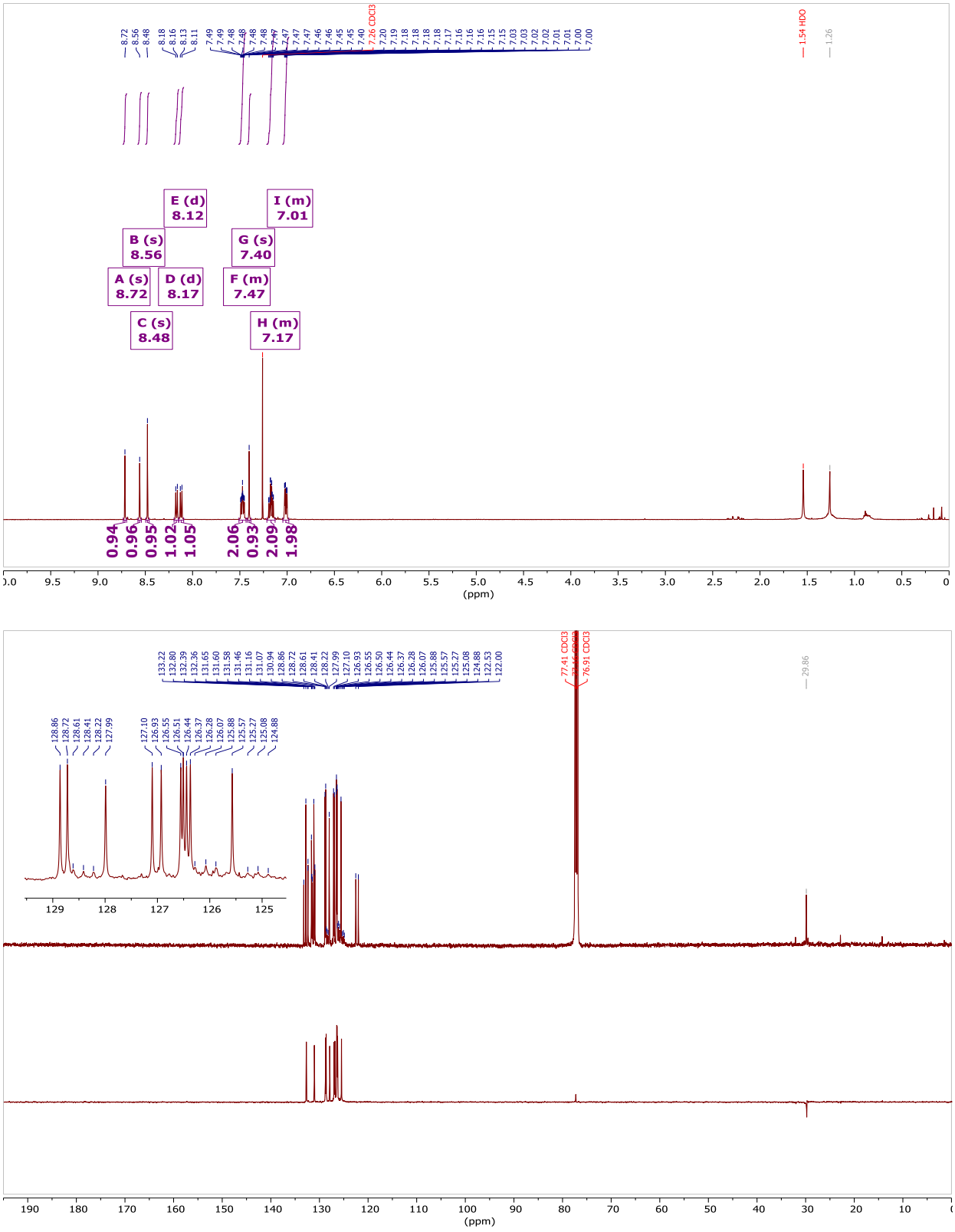

Figure S4. Top: ^{1}H NMR (500 MHz, $CDCl_3$) spectrum of (*aS*)-(**10**); bottom: $^{13}C\{^{1}H\}$ and DEPT-135 NMR (126 MHz, $CDCl_3$) spectra of (*aS*)-(**10**).

Section S2: Polarimetry

S2.1. Materials and methods

Specific optical rotations were recorded in $CHCl_3$ on an Anton Paar MCP 200 polarimeter at 25 °C, in a 10 cm (1 mL) Peltier controlled cell. $[\alpha]_D^{25}$ values are reported in degrees·mL·g^{-1}·dm^{-1} with concentration expressed in g/100 mL.

S2.2. Results

For (*aR*)-**9**, derived from (*aR*)-**11**, specific rotation $[\alpha]_D^{25}$ = +0.9(5) (*c* = 1.0, $CHCl_3$).

For (*aS*)-**9**, derived from (*aS*)-**11**, specific rotation $[\alpha]_D^{25}$ = -0.9(5) (*c* = 1.0, $CHCl_3$).

For (*aR*)-**10**, derived from (*aR*)-**11**, specific rotation $[\alpha]_D^{25}$= -1.5(5) (*c* = 0.42, $CHCl_3$).

For (*aS*)-**10**, derived from (*aS*)-**11**, specific rotation $[\alpha]_D^{25}$= +1.5(5) (*c* = 0.50, $CHCl_3$).

Section S3: Vibrational circular dichroism spectroscopy

S3.1. Materials and methods

VCD measurements

Infrared (IR) and vibrational circular dichroism (VCD) spectra were recorded using a Bruker PMA 50 accessory coupled to a Vertex 70 Fourier-transform infrared spectrometer. A Hinds PEM-90 photoelastic modulator, set to λ/4 retardation, was used to modulate the handedness of the circularly polarized light at 50 kHz, and demodulation was performed with an SR830 DSP lock-in amplifier. An optical low-pass filter (< 1800 cm^{-1}) placed before the modulator was used to improve the signal-to-noise ratio. Solid-state measurements were carried out using a cell equipped with an automated rotating sample holder.

Samples of (*aS*)-**9**, (*aR*)-**9**, (*aS*)-**10**, and (*aR*)-**10** were prepared by mixing 5.3, 5.6, 6.0, and 6.0 mg of material, respectively, with 200 mg of dry KBr for **9** and 150 mg for **10**. Two pellets were pressed from each mixture using a pelletizer under an applied pressure of approximately 7 tons. To minimize birefringence and linear dichroism artifacts, spectra were first recorded with the pellet spinning at 1.1 min^{-1} in a plane perpendicular to the incident beam. After rotating the sample holder by 180°, a second set of spectra was acquired under identical spinning conditions. For each face of each pellet, 2 h of data were accumulated. The final VCD spectrum of each enantiomer was obtained by averaging the spectra collected from both faces of both pellets. All VCD spectra were recorded at room temperature, and baseline correction was performed using the standard half-subtraction procedure applied to the two enantiomers.

For the IR absorption spectra, the empty measuring cell was used as reference, and baseline correction was performed using the elastic correction method implemented in the Bruker OPUS software.

VCD calculations

The (*aR*) enantiomer was selected for the DFT modeling of the IR and VCD spectra, with only a single conformation identified for this structure. Geometry optimizations were performed using several levels of theory, including B3LYP/6-311G(df,pd), B3LYP/6-311++G(df,pd), B3LYP-D3(BJ)/6-311G(df,pd), and M06-2X/6-311G(df,pd). While most methods converged to nearly identical geometries, the B3LYP-D3(BJ)/6-311G(df,pd) level was selected for the final analysis as it provided the best agreement with experimental IR and VCD measurements, whereas M06-2X yielded slightly less satisfactory spectral profiles. Analytical Hessian calculations were conducted at this same level to derive vibrational frequencies, IR intensities, and VCD rotational strengths. This consistency ensures compliance with the harmonic approximation by providing a vanishing gradient at the optimized coordinates. The nature of the stationary point was verified as a true local minimum via frequency analysis, confirming the absence of imaginary modes. As harmonic frequencies systematically overestimate experimental values, a scaling factor of 0.98 was applied. The simulated IR and VCD spectra were generated from the calculated dipole and rotational strengths using Lorentzian band shapes with a half-width at half-maximum of 8 cm^{-1}. All calculations were performed using Gaussian16 package.[2] All the molecular pictures were generated using AGUI from the AMPAC 11 package (http://www.semichem.com/ampac/ampacgui-features.php).

S3.2. Results

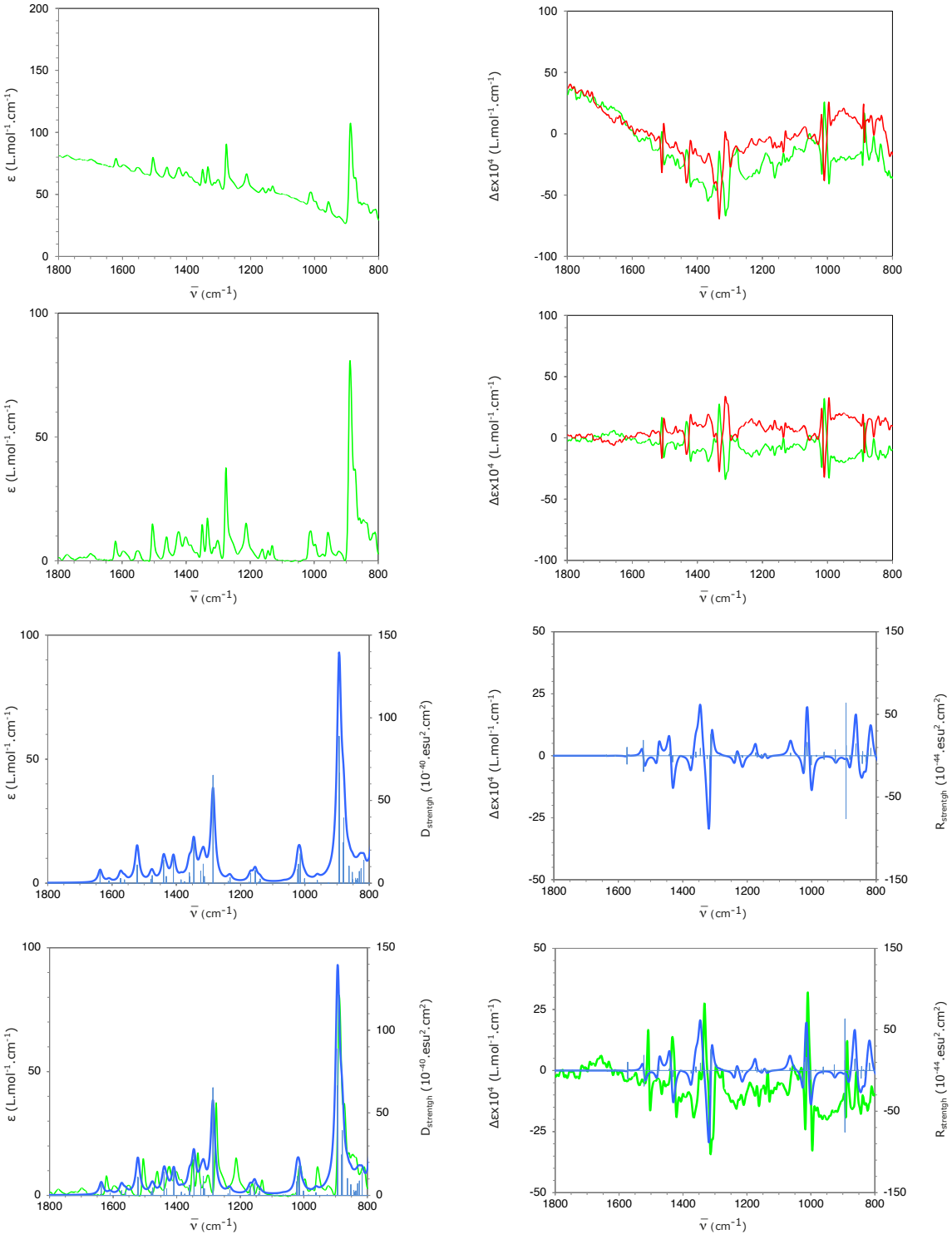

Figure S5. IR (left) and VCD (right) spectra measured for (*aR*)-**9** (green) and (*aS*)-**9** (red) sample and calculated for (*aR*)-**9** enantiomer (blue) at the B3LYP-D3(BJ)/6-311G(df,pd) level. Measured spectra are given with (first line) and without (second line) half difference baseline corrections.

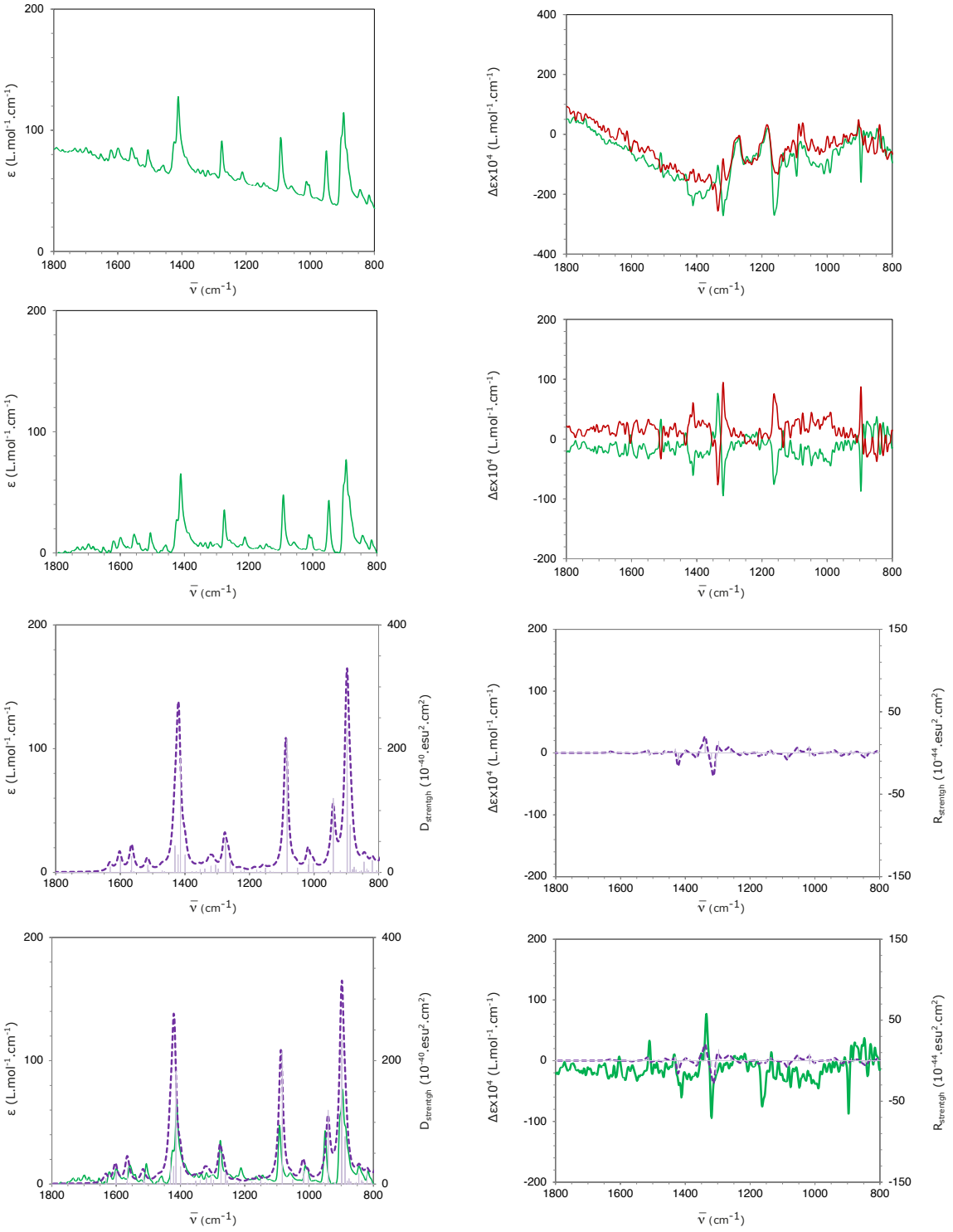

Figure S6. IR (left) and VCD (right) spectra measured for (*αR*)-**10** (dark green) and (*αS*)-**10** (dark red) sample and calculated for (*αR*)-**10** enantiomer (dashed purple) at the B3LYP-D3(BJ)/6-311G(df,pd) level. Measured spectra are given with (first line) and without (second line) half difference baseline corrections.

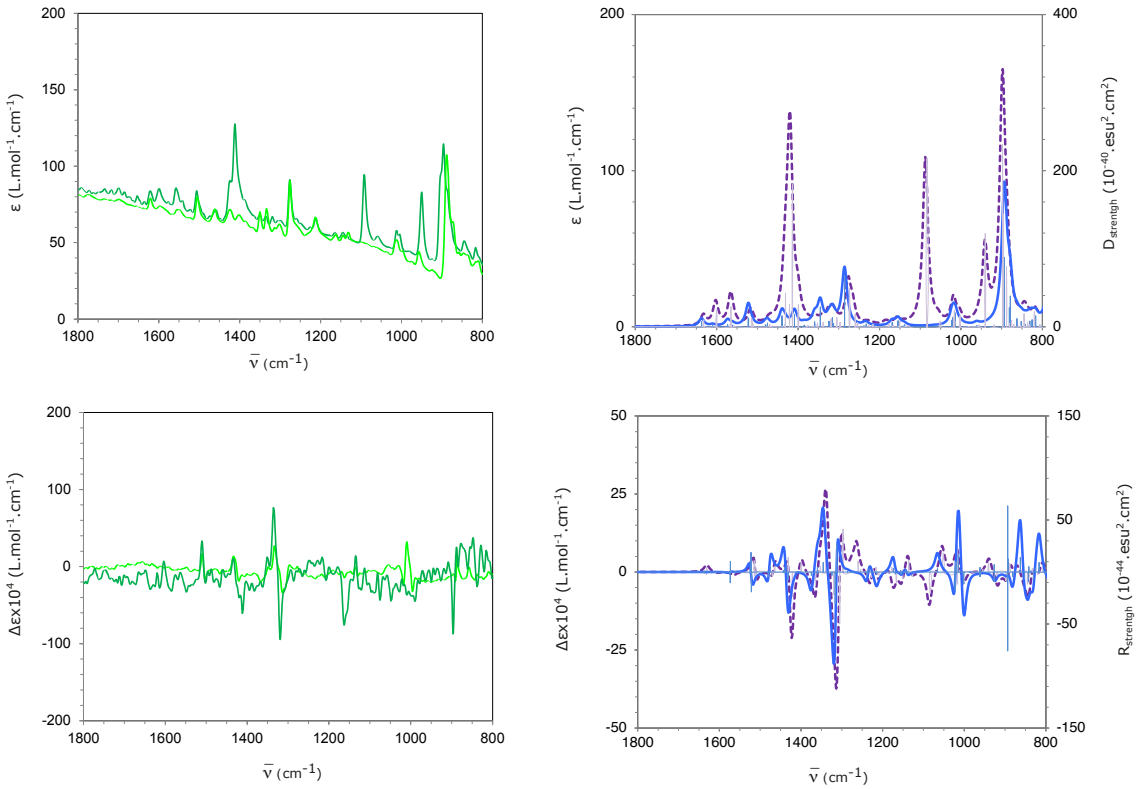

Figure S7. IR (top) and VCD (bottom) spectra measured (left) for (*aR*)-**9** (green) and (*aR*)-**10** (dark green) sample and calculated (right) for (*aR*)-**9** (blue) and (*aR*)-**10** (dashed purple) enantiomers at the B3LYP-D3(BJ)/6-311G(df,pd) level. Measured spectra are given without (first line) and with (second line) half difference baseline corrections.

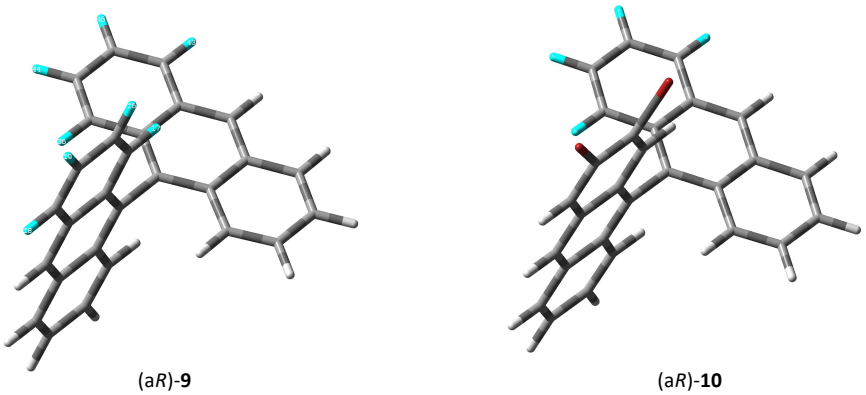

(a*R*)-**9** (a*R*)-**10**

Figure S8. Calculated geometries of (*aR*)-**9** and (*aR*)-**10** at the B3LYP-D3(BJ)/6-311G(df,pd) level. [^{2}H] atoms are shown in blue.

Table S1. Coordinates of the stationary points for the VCD study

(*aR*)-**9** Nimag = 0				(*aR*)-**10** Nimag = 0			
C	2.579453	1.472205	2.579472	Br	-3.070061	-2.344297	-0.000261
C	1.752039	0.771976	1.752050	Br	-5.067197	0.469865	-0.000187
C	0.862098	1.443162	0.862104	C	-2.327667	-0.581405	-0.000120
C	0.859655	2.882615	0.859663	C	-0.966538	-0.456487	-0.000079
C	1.741074	3.573702	1.741090	H	-0.349057	-1.343872	-0.000144
C	2.575717	2.892615	2.575739	C	-0.334668	0.822267	0.000049
C	-0.000000	0.745169	-0.000001	C	1.066976	0.959166	0.000109
C	-0.000000	3.562876	0.000001	C	1.650306	2.241528	0.000246
C	-0.859655	2.882616	-0.859662	C	3.067721	2.430246	0.000349
C	-0.862097	1.443163	-0.862105	H	3.707071	1.556708	0.000313
C	-1.752039	0.771977	-1.752052	C	3.610986	3.684337	0.000478
H	-1.759340	-0.309013	-1.759353	H	4.688089	3.806768	0.000565
C	-2.579454	1.472207	-2.579473	C	2.776810	4.837905	0.000515
C	-2.575718	2.892617	-2.575737	H	3.228258	5.823468	0.000600
C	-1.741074	3.573704	-1.741088	C	1.417576	4.703973	0.000433
H(Iso=2)	3.247804	0.944246	3.247826	H	0.776289	5.579016	0.000457
H(Iso=2)	1.759341	-0.309014	1.759349	C	0.806265	3.412633	0.000307
H(Iso=2)	1.731678	4.657077	1.731695	C	-0.581680	3.259103	0.000247
H(Iso=2)	3.240506	3.429424	3.240535	H	-1.214654	4.140689	0.000302
H	-0.000000	4.646936	0.000001	C	-1.170231	1.993186	0.000124
H	-3.247804	0.944249	-3.247828	C	-2.585665	1.826886	0.000059
H	-3.240508	3.429427	-3.240532	H	-3.214888	2.708200	0.000094
H	-1.731679	4.657078	-1.731692	C	-3.157916	0.586135	-0.000063
C	0.000000	-0.745169	-0.000001	C	1.932689	-0.259507	0.000040
C	-0.862098	-1.443162	0.862104	C	2.334890	-0.830597	-1.223498
C	0.862097	-1.443163	-0.862105	C	1.947449	-0.282711	-2.486568
C	-1.752039	-0.771976	1.752050	H	1.324643	0.602802	-2.501017
C	-0.859655	-2.882615	0.859663	C	2.350835	-0.859040	-3.658433
C	0.859655	-2.882616	-0.859662	H	2.045404	-0.428731	-4.605437
C	1.752039	-0.771977	-1.752052	C	3.170062	-2.023106	-3.651734
C	-2.579453	-1.472205	2.579472	H	3.478242	-2.465081	-4.592390
H	-1.759341	0.309014	1.759349	C	3.563633	-2.579032	-2.467862
C	-1.741074	-3.573702	1.741090	H	4.187344	-3.466713	-2.455019
C	0.000000	-3.562876	0.000001	C	3.165419	-2.010413	-1.219106
C	1.741074	-3.573704	-1.741088	C	3.557261	-2.567162	-0.000088
H(Iso=2)	1.759340	0.309013	-1.759353	H	4.181115	-3.455746	-0.000138
C	2.579454	-1.472207	-2.579473	C	3.165047	-2.010813	1.218993
C	-2.575717	-2.892615	2.575739	C	3.562864	-2.579848	2.467685
H	-3.247804	-0.944246	3.247826	H(Iso=2)	4.186549	-3.467546	2.454744
H	-1.731678	-4.657077	1.731695	C	3.168956	-2.024289	3.651618
H	0.000000	-4.646936	0.000001	H(Iso=2)	3.476821	-2.466587	4.592225
C	2.575718	-2.892617	-2.575737	C	2.349777	-0.860192	3.658445
H(Iso=2)	1.731679	-4.657078	-1.731692	H(Iso=2)	2.044102	-0.430155	4.605495
H(Iso=2)	3.247804	-0.944249	-3.247828	C	1.946756	-0.283476	2.486643
H	-3.240506	-3.429424	3.240535	H(Iso=2)	1.323987	0.602062	2.501194
H(Iso=2)	3.240508	-3.429427	-3.240532	C	2.334538	-0.830984	1.223515

Section S4: Anisotropic NMR spectroscopy

S4.1. Materials and methods

Anisotropic 1D/2D NMR spectra were recorded using Bruker NMR spectrometers, either i) a 14.1 T Avance II instrument equipped with a selective ^{2}H cryogenic probe ($\nu_{Larmor}(^2H)$ = 92.2 MHz), or ii) a 9.4 T Avance I spectrometer equipped with a BXO standard probe ($\nu_{Larmor}(^{13}C)$ = 100.4 MHz and $\nu_{Larmor}(^2H)$ = 61.3 MHz). All anisotropic 1D/2D NMR spectra recorded are ^{1}H decoupled, as noted {^{1}H}, using a basic composite pulse decoupling sequence (WALTZ-16, < 0.5 W).

S4.2. Results

The most relevant spectra are discussed in the main text (Figures 3-5); complementary 1D spectra are shown hereafter. It is assumed that the isotopic purity is identical on each site and that no ^{2}H-^{2}H coupling is observed between the deuterated sites. Both atropisotopomers **9** and **10** contain four magnetically inequivalent ^{2}H sites; accordingly, their ^{2}H-{^{1}H} 1D NMR spectra (Figure S9) show only four resonances. In the presence of the chiral liquid crystal, i.e., in their anisotropic ^{2}H-{^{1}H} 1D-NMR spectra in PBLG/$CHCl_3$, each enantiomer of atropisotopomers **9** and **10** should produce four ^{2}H quadrupolar doublets, i.e., one quadrupolar doublet for each ^{2}H site. If enantiodiscrimination is observed in the chiral polymer, then at least five and up to eight ^{2}H quadrupolar doublets should be observed for both samples *rac*-**9** and *rac*-**10**. In Figure S10, the anisotropic ^{2}H-{^{1}H} 1D NMR spectrum of *rac*-**9** in PBLG/$CHCl_3$ shows only four ^{2}H quadrupolar doublets, indicating that no enantiodiscrimination occurs in this case. In Figure S11, the anisotropic ^{2}H-{^{1}H} 1D NMR spectrum of *rac*-**10** in PBLG/$CHCl_3$ shows six ^{2}H quadrupolar doublets, indicating that enantiodiscrimination occurs at two ^{2}H sites in this case. Both anisotropic ^{2}H-{^{1}H} 1D NMR spectra of (*aR*)-**10** and (*aS*)-**10** in PBLG/$CHCl_3$ (Figure S12) show only four ^{2}H quadrupolar doublets, indicating that a single enantiomer is detected in each sample. An example of anisotropic ^{13}C-{^{1}H} 1D NMR is provided in Figure S13 for (*aR*)-**10**.

On the ^{2}H *Q*-COSY Fz 2D experiments show in Figure 3 of the main text, the ^{2}H chemical shifts and ^{2}H quadrupolar doublets evolve simultaneously during the t_1 and t_2 periods of the sequence, and so appear in the F_1 and F_2 dimensions after a double Fourier transformation. As in the case of ^{2}H *Q*-resolved 2D spectra in Figure 4 of the main text, the absence of diagonal peaks allows to apply a 45° tilt process ('tilt' command in the Bruker Topspin software). This leads to: (i) displaying the ^{2}H chemical shifts and ^{2}H quadrupolar doublets in the F_1 vertical dimension in ppm to measure $d(^2H)$ (center of quadrupolar doublet) for each magnetically non-equivalent deuteron; (ii) formally removing the ^{2}H-QDs in F_2 horizontal dimension and thus leading to a 'pure-shift' type spectrum in ppm.

In Figure 4 in the main text, only ^{2}H quadrupolar doublets appear in the F_1 vertical dimension. A scale in Hz is therefore pertinent to measure ^{2}H quadrupolar splitting in F_1. Application of a 45° tilt process ('tilt' command in the Bruker Topspin software) allows formally removing the ^{2}H quadrupolar doublets, hence only the ^{2}H chemical shifts (one peak per magnetically non-equivalent deuterated site) appear in F_2 dimension. A scale in ppm is therefore pertinent to measure ^{2}H chemical shifts in the F_2 dimension. The visualization of doublets and their analysis is therefore simple.

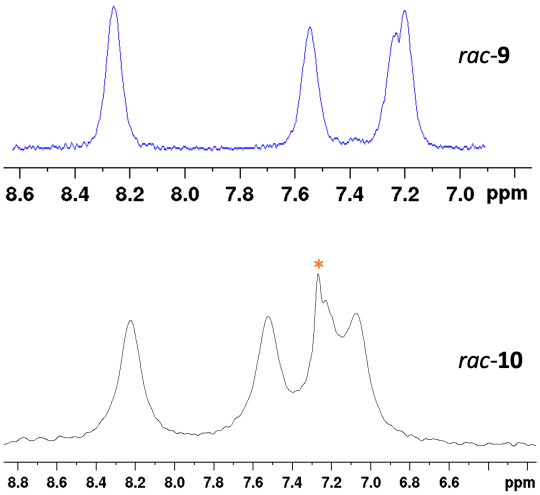

Figure S9. ^{2}H-{^{1}H} 1D-NMR spectrum of *rac*-**9** (top, 92.2 MHz, 310 K) and *rac*-**10** (bottom, 61.3 MHz, 305 K) in $CHCl_3$. The resonance noted * corresponds to the natural abundance of ^{2}H in chloroform.

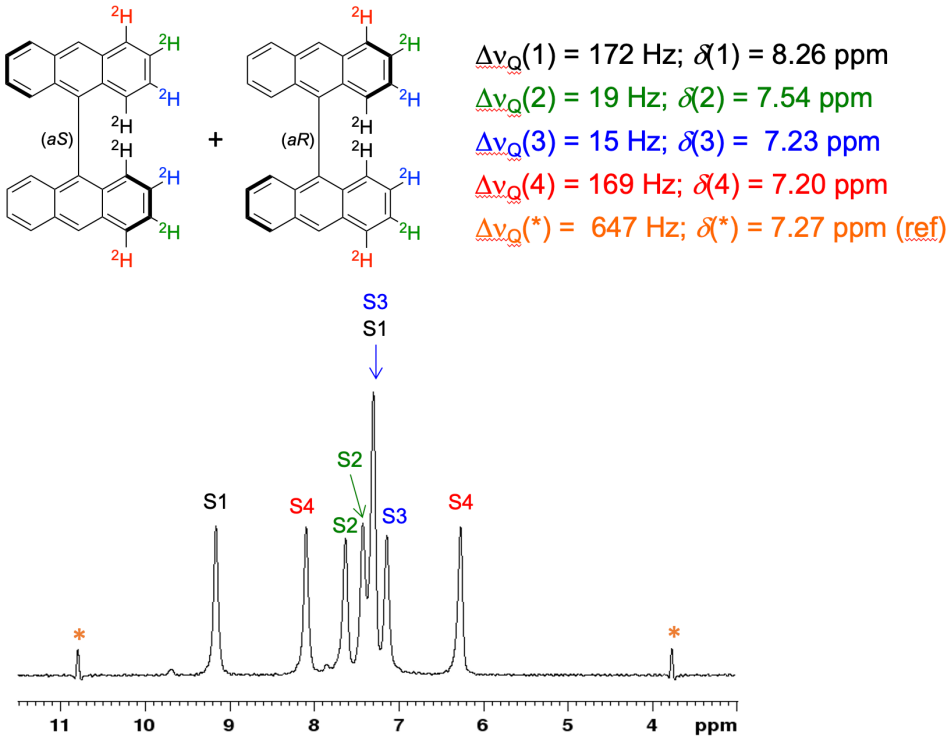

Figure S10. Anisotropic ^{2}H-{^{1}H} 1D-NMR spectrum of *rac*-**9** in PBLG/$CHCl_3$ (92.2 MHz, 310 K). The resonance noted with * corresponds to the natural abundance of ^{2}H in $CHCl_3$.

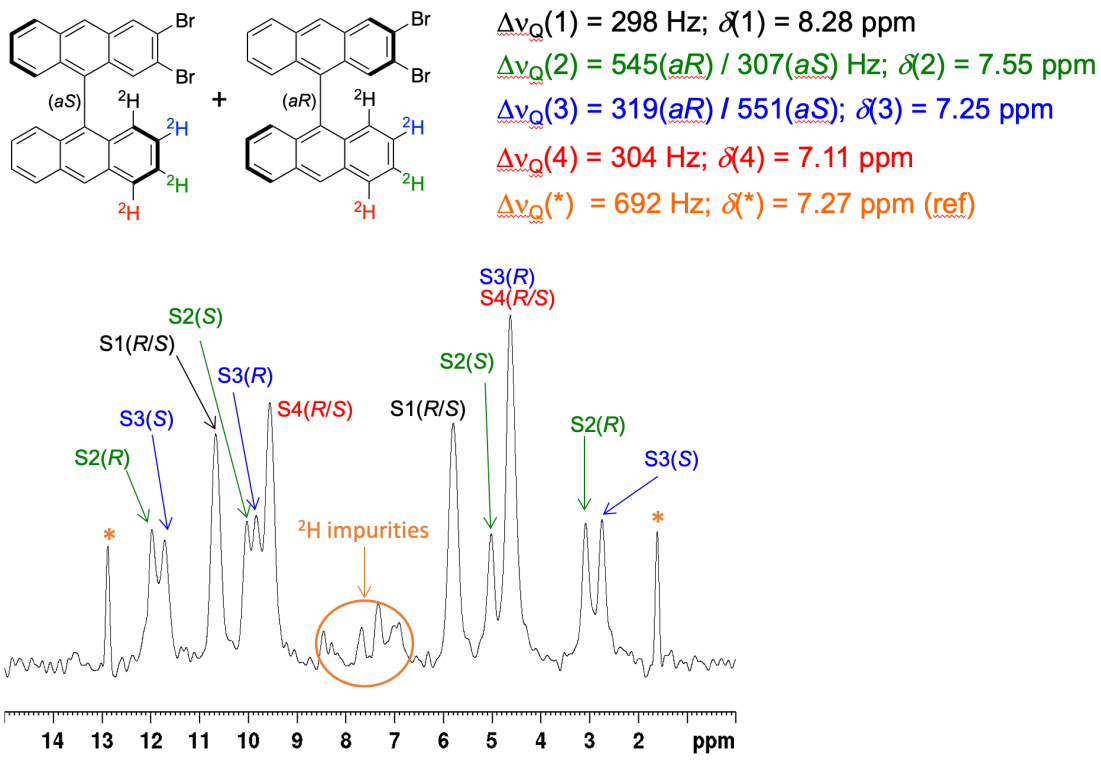

Figure S11. Anisotropic ^{2}H-{^{1}H} 1D-NMR spectrum of *rac*-**10** in PBLG/$CHCl_3$ (61.3 MHz, 305 K, 10 000 scans). The resonance noted with * corresponds to the natural abundance of ^{2}H in $CHCl_3$. The sample of *rac*-**10** was contaminated by some ^{2}H-containing impurities.

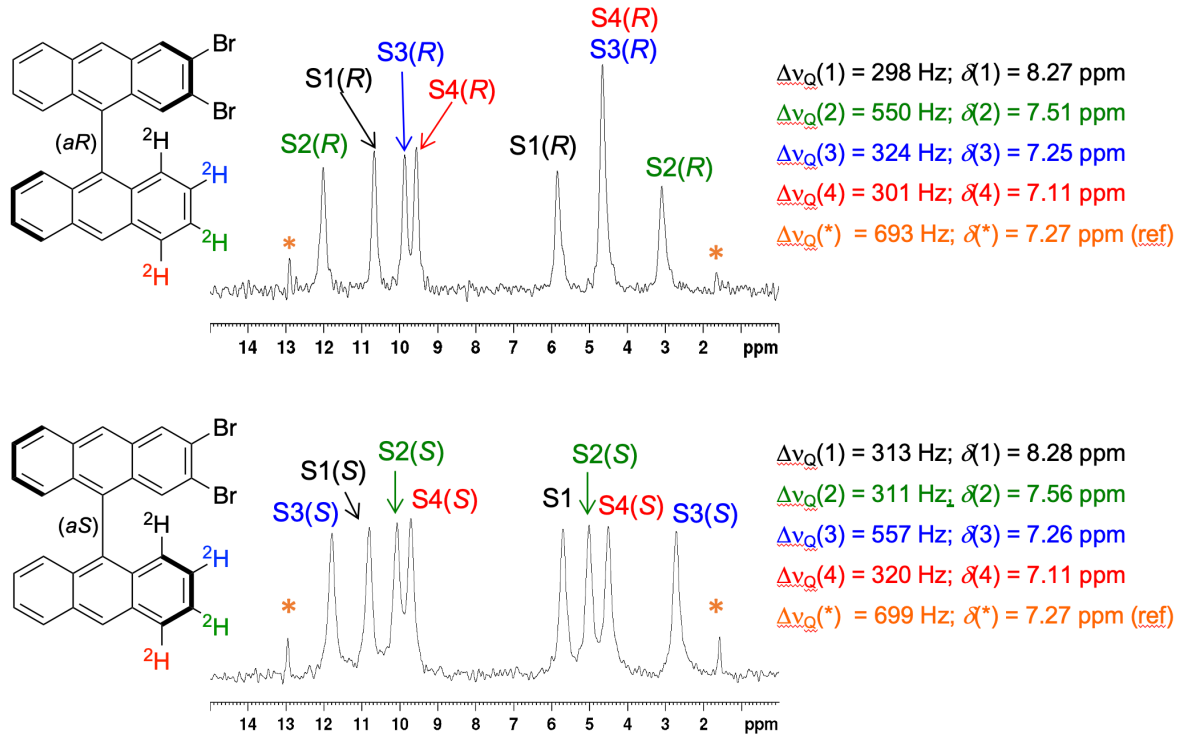

Figure S12. Anisotropic ^{2}H-{^{1}H} 1D-NMR spectra of (*aR*)-**10** (top, 61.3 MHz, 305 K, 10 000 scans) and (*aS*)-**10** (bottom, 61.3 MHz, 305 K, 10 000 scans) in PBLG/$CHCl_3$. The resonances noted with * correspond to the natural abundance of ^{2}H in $CHCl_3$.

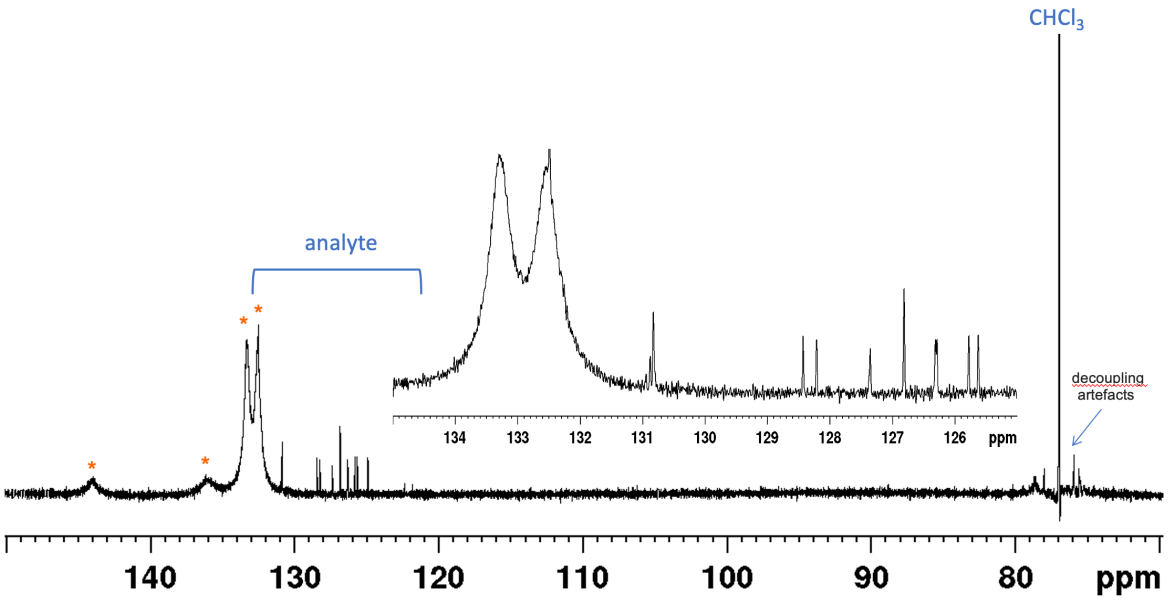

Figure S13. Anisotropic ^{13}C-{^{1}H} 1D-NMR spectrum of (*aR*)-**10** (100.4 MHz, 305 K) in PBLG/$CHCl_3$. The resonances noted with * correspond to the PBLG polymer.

Section S5: Theoretical determination of the rotation barrier in 9,9'-bianthryl

S5.1. Materials and methods

Geometries of the stationary points were optimized without symmetry constraints with the Gaussian 16 program[2] using the DFT PBE0 hybrid functional[3] and the def2-TZVP basis set[4] in the gas phase. The D3 Grimme energy corrections for dispersion with the Becke-Johnson damping function were added in all calculations.[5] Analytical Hessians were computed to determine the nature of stationary points: one and zero imaginary frequencies (Nimag) for transition states and minima, respectively, and to calculate unscaled zero-point energies (ZPE) as well as thermal corrections and entropy effects using the standard statistical-mechanics relationships for an ideal gas.[6] These two latter terms were computed at 298.15 K and 1 atm to provide the reported relative Gibbs energies. As a summary, the reported Gibbs energies were calculated at the PBE0-D3(BJ)/def2-TZVP level at 298.15 K and 1 atm.

S5.2. Results

While the rotation process around the C(sp^2)–C(sp^2) single bond in small biaryls is typically a single step process (i.e., occurring without intermediate), it was found that the rotation process around the C(sp^2)–C(sp^2) single bond in 9,9'-bianthryl is a symmetric two-step process occurring via the high-energy unstable intermediate **INT** with C_i symmetry (Fig S14). Each anthryl fragment in intermediate **INT** shows a negative curvature (Fig S15). Overall, the rotation barrier around the C(sp^2)–C(sp^2) single bond in 9,9'-bianthryl was evaluated at 185.0 kJ mol^{-1}. Using the Eyring equation, this corresponds to rotation half-times $t_{1/2}$(rot) ≈ 10^{12} years at 298 K and $t_{1/2}$(rot) > 600 years at 413 K. The coordinates of the stationary points are provided in Table S2.

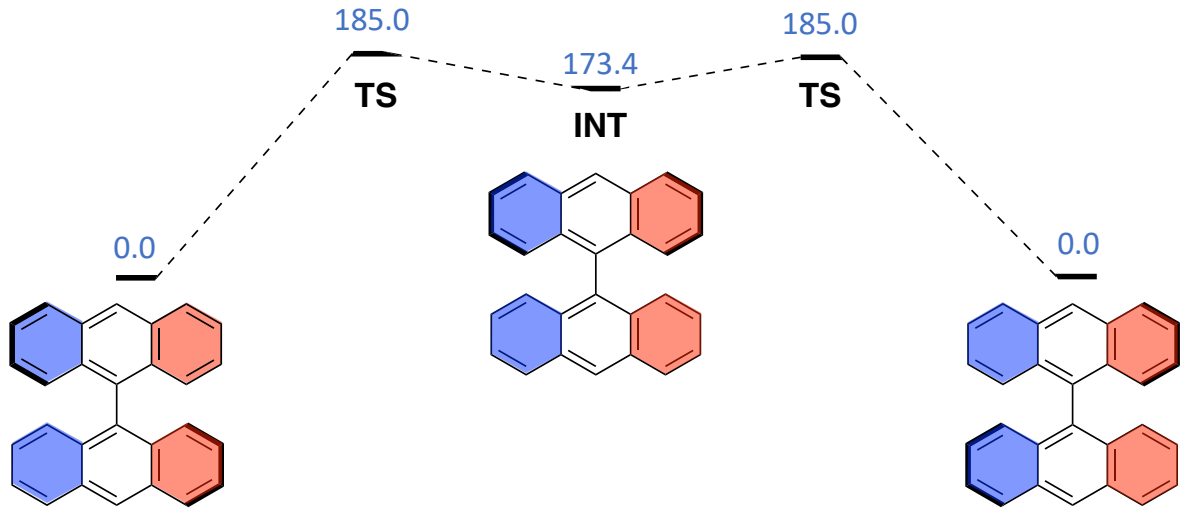

Figure S14. Energy diagram of the rotation process around the C(sp^2)–C(sp^2) single bond in 9,9'-bianthryl calculated at the DFT PBE0-D3(BJ)/def2-TZVP. Gibbs energies in kJ mol^{-1} at 298 K and 1 atm.

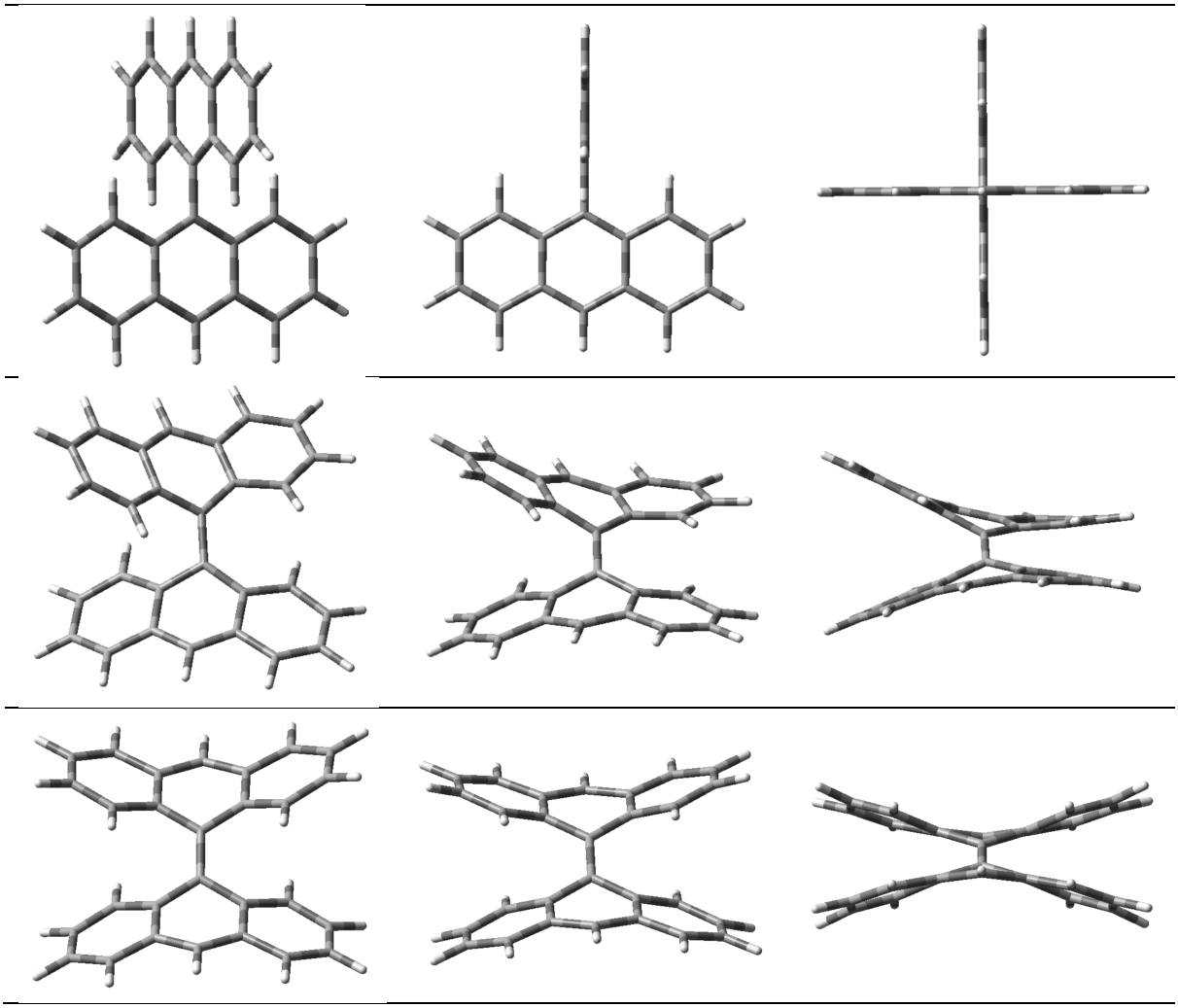

Figure S15. Representations of 9,9'-bianthryl (top), the transition state **TS** (middle) and the intermediate **INT** (bottom).

Table S2. Coordinates of the stationary points for the conformational analysis

9,9'-bianthryl				**TS**				**INT**			
Nimag = 0				Nimag = 1				Nimag = 0			
Sum of electronic and thermal Free				Sum of electronic and thermal Free				Sum of electronic and thermal Free			
Energies= -1076.690455				Energies= -1076.620006				Energies= -1076.624413			
C	-3.66900	3.25700	-0.66300	C	-3.66900	3.25700	-0.66300	C	2.56900	2.88500	2.56900
C	-3.96600	1.93700	-0.80000	C	-3.96600	1.93700	-0.80000	C	1.73600	3.56500	1.73600
C	-3.03700	0.92700	-0.43300	C	-3.03700	0.92700	-0.43300	C	0.85700	2.87400	0.85700
C	-1.69400	1.29100	-0.07200	C	-1.69400	1.29100	-0.07200	C	0.86000	1.44100	0.86000
C	-1.48400	2.67100	0.17800	C	-1.48400	2.67100	0.17800	C	1.74700	0.77000	1.74700
C	-2.43000	3.61800	-0.09600	C	-2.43000	3.61800	-0.09600	C	2.57300	1.46800	2.57300
C	-3.45500	-0.39600	-0.34800	C	-3.45500	-0.39600	-0.34800	C	-0.00000	3.55400	0.00000
C	-0.73000	0.24800	0.11700	C	-0.73000	0.24800	0.11700	C	-0.00000	0.74300	0.00000
C	-1.28400	-0.99800	0.55700	C	-1.28400	-0.99800	0.55700	C	-0.86000	1.44000	-0.86000
C	-2.64500	-1.33700	0.26700	C	-2.64500	-1.33700	0.26700	C	-0.85700	2.87400	-0.85700
C	-3.14200	-2.62300	0.61700	C	-3.14200	-2.62300	0.61700	C	-1.73600	3.56400	-1.73600
H	-4.16300	-2.86700	0.34400	H	-4.16300	-2.86700	0.34400	H	-1.72600	4.64900	-1.72600
C	-2.37800	-3.50200	1.31700	C	-2.37800	-3.50200	1.31700	C	-2.56900	2.88500	-2.56900
C	-1.07300	-3.12800	1.71500	C	-1.07300	-3.12800	1.71500	C	-2.57300	1.46800	-2.57300
C	-0.54400	-1.93300	1.33400	C	-0.54400	-1.93300	1.33400	C	-1.74700	0.77000	-1.74700
H	-4.46000	-0.66300	-0.66000	H	-4.46000	-0.66300	-0.66000	H	-0.00000	4.63900	-0.00000
H	-4.39700	4.01800	-0.91800	H	-4.39700	4.01800	-0.91800	H	3.23400	3.42400	3.23400
H	-4.94800	1.62200	-1.13600	H	-4.94800	1.62200	-1.13600	H	1.72600	4.64900	1.72600
H	-0.59200	2.97400	0.69800	H	-0.59200	2.97400	0.69800	H	1.75300	-0.31300	1.75300
H	-2.23400	4.65300	0.15800	H	-2.23400	4.65300	0.15800	H	3.24200	0.93900	3.24100
H	-2.77300	-4.47100	1.59900	H	-2.77300	-4.47100	1.59900	H	-3.23400	3.42400	-3.23400
H	-0.48900	-3.79600	2.33700	H	-0.48900	-3.79600	2.33700	H	-3.24200	0.93900	-3.24100
H	0.45400	-1.66900	1.65400	H	0.45400	-1.66900	1.65400	H	-1.75300	-0.31300	-1.75300
C	3.66900	3.25700	0.66300	C	3.66900	3.25700	0.66300	C	-2.56900	-2.88500	2.56900
C	3.96600	1.93700	0.80000	C	3.96600	1.93700	0.80000	C	-1.73600	-3.56500	1.73600
C	3.03700	0.92700	0.43300	C	3.03700	0.92700	0.43300	C	-0.85700	-2.87400	0.85700
C	1.69400	1.29100	0.07200	C	1.69400	1.29100	0.07200	C	-0.86000	-1.44100	0.86000
C	1.48400	2.67100	-0.17800	C	1.48400	2.67100	-0.17800	C	-1.74700	-0.77000	1.74700
C	2.43000	3.61800	0.09600	C	2.43000	3.61800	0.09600	C	-2.57300	-1.46800	2.57300
C	3.45500	-0.39600	0.34800	C	3.45500	-0.39600	0.34800	C	0.00000	-3.55400	0.00000
C	0.73000	0.24800	-0.11700	C	0.73000	0.24800	-0.11700	C	0.00000	-0.74300	0.00000
C	1.28400	-0.99800	-0.55700	C	1.28400	-0.99800	-0.55700	C	0.86000	-1.44000	-0.86000
C	2.64500	-1.33700	-0.26700	C	2.64500	-1.33700	-0.26700	C	0.85700	-2.87400	-0.85700
C	3.14200	-2.62300	-0.61700	C	3.14200	-2.62300	-0.61700	C	1.73600	-3.56400	-1.73600
H	4.16300	-2.86700	-0.34400	H	4.16300	-2.86700	-0.34400	H	1.72600	-4.64900	-1.72600
C	2.37800	-3.50200	-1.31700	C	2.37800	-3.50200	-1.31700	C	2.56900	-2.88500	-2.56900
C	1.07300	-3.12800	-1.71500	C	1.07300	-3.12800	-1.71500	C	2.57300	-1.46800	-2.57300
C	0.54400	-1.93300	-1.33400	C	0.54400	-1.93300	-1.33400	C	1.74700	-0.77000	-1.74700
H	4.46000	-0.66300	0.66000	H	4.46000	-0.66300	0.66000	H	0.00000	-4.63900	-0.00000
H	4.39700	4.01800	0.91800	H	4.39700	4.01800	0.91800	H	-3.23400	-3.42400	3.23400
H	4.94800	1.62200	1.13600	H	4.94800	1.62200	1.13600	H	-1.72600	-4.64900	1.72600
H	0.59200	2.97400	-0.69800	H	0.59200	2.97400	-0.69800	H	-1.75300	0.31300	1.75300
H	2.23400	4.65300	-0.15800	H	2.23400	4.65300	-0.15800	H	-3.24200	-0.93900	3.24100
H	2.77300	-4.47100	-1.59900	H	2.77300	-4.47100	-1.59900	H	3.23400	-3.42400	-3.23400
H	0.48900	-3.79600	-2.33700	H	0.48900	-3.79600	-2.33700	H	3.24200	-0.93900	-3.24100
H	-0.45400	-1.66900	-1.65400	H	-0.45400	-1.66900	-1.65400	H	1.75300	0.31300	-1.75300

Section S6: References

1 G. Dauvergne, J.-V. Naubron, M. Giorgi, X. Bugaut, J. Rodriguez, Y. Carissan and Y. Coquerel, Enantiospecific Synthesesof Congested Atropisomers through Chiral Bis(aryne)Synthetic Equivalents, *Chem. Eur. J.*, 2022, **2022**, e202202473.

2 Gaussian 16, Revision A.03, M. J. Frisch, G. W. Trucks, H. B. Schlegel, G. E. Scuseria, M. A. Robb, J. R. Cheeseman, G. Scalmani, V. Barone, G. A. Petersson, H. Nakatsuji, X. Li, M. Caricato, A. V. Marenich, J. Bloino, B. G. Janesko, R. Gomperts, B. Mennucci, H. P. Hratchian, J. V. Ortiz, A. F. Izmaylov, J. L. Sonnenberg, D. Williams-Young, F. Ding, F. Lipparini, F. Egidi, J. Goings, B. Peng, A. Petrone, T. Henderson, D. Ranasinghe, V. G. Zakrzewski, J. Gao, N. Rega, G. Zheng, W. Liang, M. Hada, M. Ehara, K. Toyota, R. Fukuda, J. Hasegawa, M. Ishida, T. Nakajima, Y. Honda, O. Kitao, H. Nakai, T. Vreven, K. Throssell, J. A. Montgomery, Jr., J. E. Peralta, F. Ogliaro, M. J. Bearpark, J. J. Heyd, E. N. Brothers, K. N. Kudin, V. N. Staroverov, T. A. Keith, R. Kobayashi, J. Normand, K. Raghavachari, A. P. Rendell, J. C. Burant, S. S. Iyengar, J. Tomasi, M. Cossi, J. M. Millam, M. Klene, C. Adamo, R. Cammi, J. W. Ochterski, R. L. Martin, K. Morokuma, O. Farkas, J. B. Foresman and D. J. Fox, Gaussian, Inc., Wallingford CT, 2016.

3 C. Adamo and V. Barone, Toward reliable density functional methods without adjustable parameters: The PBE0 model, *J. Chem. Phys.*, 1999, **110**, 6158.

4 (a) F. Weigend and R. Ahlrichs, Balanced basis sets of split valence, triple zeta valence and quadruple zeta valence quality for H to Rn: Design and assessment of accuracy, *Phys. Chem. Chem. Phys.*, 2005, **7**, 3297; (b) F. Weigend, Accurate Coulomb-fitting basis sets for H to Rn, *Phys. Chem. Chem. Phys.*, 2006, **8**, 1057.

5 S. Grimme, S. Ehrlich and L. Goerigk, Effect of the damping function in dispersion corrected density functional theory, *J. Comp. Chem.*, 2011, **32**, 1456.

6 P. Atkins, J. de Paula and J. Keeler, Atkins' Physical Chemistry, Oxford University Press, Oxford, 2022.